Nanoscale Horizons

COMMUNICATION

View Article Online
View Journal | View Issue

Cite this: *Nanoscale Horiz.*, 2020, 5, 507

Received 1st May 2019,
Accepted 14th August 2019

DOI: 10.1039/c9nh00286c

rsc.li/nanoscale-horizons

Safer-by-design biocides made of tri-thiol bridged silver nanoparticle assemblies†

Marianne Marchioni, [a] Giulia Veronesi, [ab] Isabelle Worms, [‡ac] Wai Li Ling, [d] Thomas Gallon, [ae] Didier Leonard, [f] Christelle Gateau, [e] Mireille Chevallet, [a] Pierre-Henri Jouneau, [g] Laura Carlini, [h] Chiara Battocchio, [h] Pascale Delangle, [e] Isabelle Michaud-Soret *[a] and Aurélien Deniaud *[a]

Silver nanoparticles (AgNPs) are efficient biocides increasingly used in consumer products and medical devices. Their activity is due to their capacity to release bioavailable Ag(I) ions making them long-lasting biocides but AgNPs themselves are usually easily released from the product. Besides, AgNPs are highly sensitive to various chemical environments that triggers their transformation, decreasing their activity. Altogether, widespread use of AgNPs leads to bacterial resistance and safety concerns for humans and the environment. There is thus a crucial need for improvement. Herein, a proof of concept for a novel biocide based on AgNP assemblies bridged together by a tri-thiol bioinspired ligand is presented. The final nanomaterial is stable and less sensitive to chemical environments with AgNPs completely covered by organic molecules tightly bound *via* their thiol functions. Therefore, these AgNP assemblies can be considered as safer-by-design and innovative biocides, since they deliver a sufficient amount of Ag(I) for biocidal activity with no release of AgNPs, which are insensitive to transformations in the nanomaterial.

New concepts

A new concept of mesoscopic materials with nano-properties is developed. It consists of an assembly of silver nanoparticles bridged together by a bio-inspired molecule covalently bonded to the nanoparticle surface through its three thiol functions. This results in a material that can release silver ions in a slow and controlled manner, in contrast to the existing nano-enabled biocides currently employed in consumer products and medical devices, in which silver nanoparticles undergo uncontrolled release. Thus, silver nanoparticle assemblies can be the building blocks of future nano-enabled biocides conceived from a safer-by-design perspective, where the amount of released ions is reduced to an amount required to kill bacteria, while avoiding unnecessary Ag leaching from the nanoparticle. The proof of concept of the self-assembly process and surface science insights into the assembly mechanism are provided, as well as the demonstration of the biocidal activity of the resulting nanomaterial.

Introduction

Silver nanoparticles (AgNPs) are widely used in consumer products due to their biocidal activity. AgNP-containing medical devices are also a growing market with applications in dentistry, prosthesis, catheters or wound dressings. Their action is due to Ag(I) release that is highly toxic for microorganisms inducing alterations of lipid bilayers, proteins and nucleic acids. This wide spectrum of effects makes them a good choice to avoid specific mutations in bacterial strains that could confer resistance. However, resistant strains have been observed[1] thanks to acquisition of the ability to chelate and excrete or to trap Ag species.[2–4] The reactivity of Ag in general and AgNPs in particular is very complex and depends on the surrounding media[5] including living species such as *Bacillus subtilis* that secretes molecules to hinder their activity.[6] Ag(I) release from AgNPs is based on an oxidative dissolution mechanism and thus requires oxygen.[7] In aerobiosis, the metallic Ag(0) core of AgNPs is covered with surface Ag(I) species, and the dissolution of the NP into ions is favored by pH decrease[8] and/or by some thiol molecules.[9,10] The behavior of AgNPs in the presence of thiol molecules is highly versatile either inducing time-dependent dissolution into ions[9,10] or forming a coating that protects the NP.[8,11] These phenomena depend on the architecture of the molecules and the number of thiols[8,9,11] but have remained unpredictable to date. In order to solve the issues about NP use, next generation

[a] *Univ. Grenoble Alpes, CNRS, CEA, IRIG, Laboratoire de Chimie et Biologie des Métaux, 38000 Grenoble, France. E-mail: aurelien.deniaud@cea.fr, isabelle.michaud-soret@cea.fr; Tel: +33 4 38 78 96 51, +33 4 38 78 99 40*
[b] *ESRF, The European Synchrotron, 71 Avenue des Martyrs, 38000 Grenoble, France*
[c] *Univ. Grenoble Alpes, CEA, LITEN/DTNM/SEN/L2N, F-38054 Grenoble Cedex 09, France*
[d] *Univ. Grenoble Alpes, CEA, CNRS, IBS, F-38000 Grenoble, France*
[e] *Univ. Grenoble Alpes, CEA, CNRS, IRIG, SyMMES, 38000 Grenoble, France*
[f] *Univ. Lyon, CNRS, Université Claude Bernard Lyon 1, Institut des Sciences Analytiques, UMR 5280, 5, rue de la Doua, F-69100 Villeurbanne, France*
[g] *Univ. Grenoble Alpes, CEA, IRIG, MEM, 38000 Grenoble, France*
[h] *Univ. Roma Tre, Dept. of Sciences, Via della Vasca Navale 79, 00146 Rome, Italy*
† Electronic supplementary information (ESI) available: See DOI: 10.1039/c9nh00286c
‡ Present address: Department F.-A. Forel for Environmental and Aquatic Sciences, University of Geneva, 66 Boulevard Carl Vogt CH-1211 Geneva 4, Switzerland.

nanomaterials are being developed following a safer-by-design approach.[12] In the case of AgNPs, it is crucial to limit Ag(I) release to the strictly required amount for the biocidal activity. Besides, it would also be interesting to avoid AgNP release from the product in the environment or in the human body for medical devices. This approach would therefore limit bacterial resistance against silver and toxicity for mammals and other living species. In order to reach these objectives, we developed an innovative strategy that consists in bridging AgNPs together using a tri-thiol molecule, which favors the formation of larger and stable species that are called AgNP assemblies. In these assemblies, AgNPs retain their high specific surface area without being released from the final product. The growth of the AgNP assemblies is mediated by thiol functions and can be controlled using a thiol-reactive molecule to stop the process and thereby to obtain a stable nanomaterial of defined size. Hence, AgNPs are entrapped into a tightly bound organic coating, which enables the long-lasting, slow dissolution into Ag(I). Therefore, the release from AgNP assemblies is reduced to an amount necessary to retain the biocidal activity, unlike isolated AgNPs, which undergo uncontrolled ion release. Altogether, using a smart and innovative process we reached the objectives needed for the future production of safer biocides to be grafted on nano-enabled biocidal products.

Results and discussion

$NTA(CysOEt)_3$, abbreviated as L^{3S} in the following, is a tri-thiol molecule with C_3 symmetry inspired from a single metallothionein Cu(I) binding site (Fig. 1a).[13] This is a high affinity ligand for Cu(I) and Ag(I) that forms AgS_3 complexes.[14] In the presence of 20 nm diameter citrate-coated AgNPs in equimolar concentration of Ag and S, L^{3S} induced a change in the solution color over time (Fig. 1b), due to a modification of the surface plasmon resonance (SPR) properties (Fig. 1c). Indeed, a decrease of the specific AgNP SPR signal around 400 nm was observed, along with the appearance of a broad peak centered at higher wavelengths that increased with time. This phenomenon is explained by the formation of a non-symmetric dipole and is due to nanoparticles in contact without interpenetration between them.[15] These results suggested that L^{3S} induced an AgNP agglomeration-like mechanism, which is confirmed by the time-dependent increase of the hydrodynamic diameter of the species in solution, reaching about 250 nm with a homogeneous distribution after 1 h of reaction and more than 1 μm in a heterogeneous distribution after 75 min (Fig. 1d). However, several pieces of experimental evidence allow us to rule out the occurrence of simple agglomeration, meant as the formation of clusters of NPs held together by weak physical interactions in an unpredictable way, resulting in a bulk material with no nano-properties.

Thiol molecules were previously demonstrated to favor AgNP dissolution into Ag(I) soluble species with kinetics increasing with the number of thiol per molecule.[9] Indeed, phytochelatin-3, a tri-thiol molecule, induced an almost four times faster dissolution than glutathione, our standard one thiol molecule. Surprisingly, similar experiments performed with the tri-thiol molecule L^{3S} showed a slightly slower AgNP dissolution compared to the reaction with glutathione leading to a lower amount of Ag(I) released after 24 h incubation (Fig. 1e). In order to have a complete view of the different species produced over time, asymmetrical flow-field flow-fractionation (AF_4) experiments were performed with online detection of Ag by inductively coupled plasma–mass spectrometry (ICP-MS) (Fig. 1f). Pristine AgNPs alone were eluted at 15 min retention time and remained stable in solution over 24 h. The incubation with L^{3S} led to (i) the decrease of the AgNP peak (15 min) over time, (ii) the appearance of a peak at lower retention time around 11 min that corresponded to Ag(I) soluble species and (iii) the appearance of a broad peak corresponding to assemblies at a higher retention time, the latter increasing with the incubation duration. These results highlight the time-dependent formation of large assemblies of AgNPs triggered by L^{3S}. Moreover, the kinetics of the process can gradually be slowed down by decreasing the S to Ag molar ratio to 0.25 and 0.05, as shown by SPR spectra and dynamic light scattering (DLS) distributions (Fig. S1, ESI†). To control the assembly process, further experiments were performed with an S to Ag molar ratio of 0.25 and using iodoacetamide, a thiol-reactive molecule that alkylates and blocks free thiol functions. When added after 1 h of incubation between AgNPs and L^{3S}, the evolution of both SPR spectra and DLS distributions was stopped and the assemblies were stable for at least 120 h at 25 °C (Fig. 2a, b *vs.* Fig. 1c, d). This proves that the AgNP assembly is thiol-driven and is not an agglomeration mechanism, which would be insensitive to iodoacetamide but sensitive to dilution, as observed with oxidized glutathione (Fig. S2, ESI†).

In order to prepare assemblies of different sizes, L^{3S} and AgNPs were incubated for 1 hour before addition of iodoacetamide. Thiol-blocked AgNP assemblies were then fractionated using discontinuous sucrose gradient centrifugation into assemblies of different average hydrodynamic diameters (Fig. 2c). We obtained populations of assemblies of 40, 60 and 200 nm based on DLS measurement with different SPR spectra and colors (Fig. S3, ESI†) and zeta potentials of −28.3, −21.0 and −24.8 mV for the assemblies of 40, 60 and 200 nm, respectively. The DLS diameter distributions showed a clear shift towards larger diameter for the main peak but a second low intensity peak was observed at smaller values for both 60 and 200 nm assemblies (Fig. 2c). Therefore, the diameters determined by DLS are not accurate and the values 40, 60 and 200 nm are used as labels of the different populations of assemblies in the following. The morphology of the assemblies and the number of particles per assembly were analyzed by electron microscopy: scanning transmission electron microscopy (STEM) and cryo-transmission electron microscopy (cryo-TEM) (Fig. S4, ESI,† and Fig. 2d). Despite the different preparation protocols, both techniques clearly showed clusters of AgNPs comprising a number of NPs that increased with the expected size of the assemblies. Statistical analysis (Fig. S4b, ESI†) showed that 40 nm assemblies are mainly formed by 1 to 4 NPs, 60 nm assemblies contained between 5 and 40 NPs with most assemblies containing 15 NPs and 200 nm assemblies are made of 16 to 60 NPs with most assemblies containing 40. Indeed, the

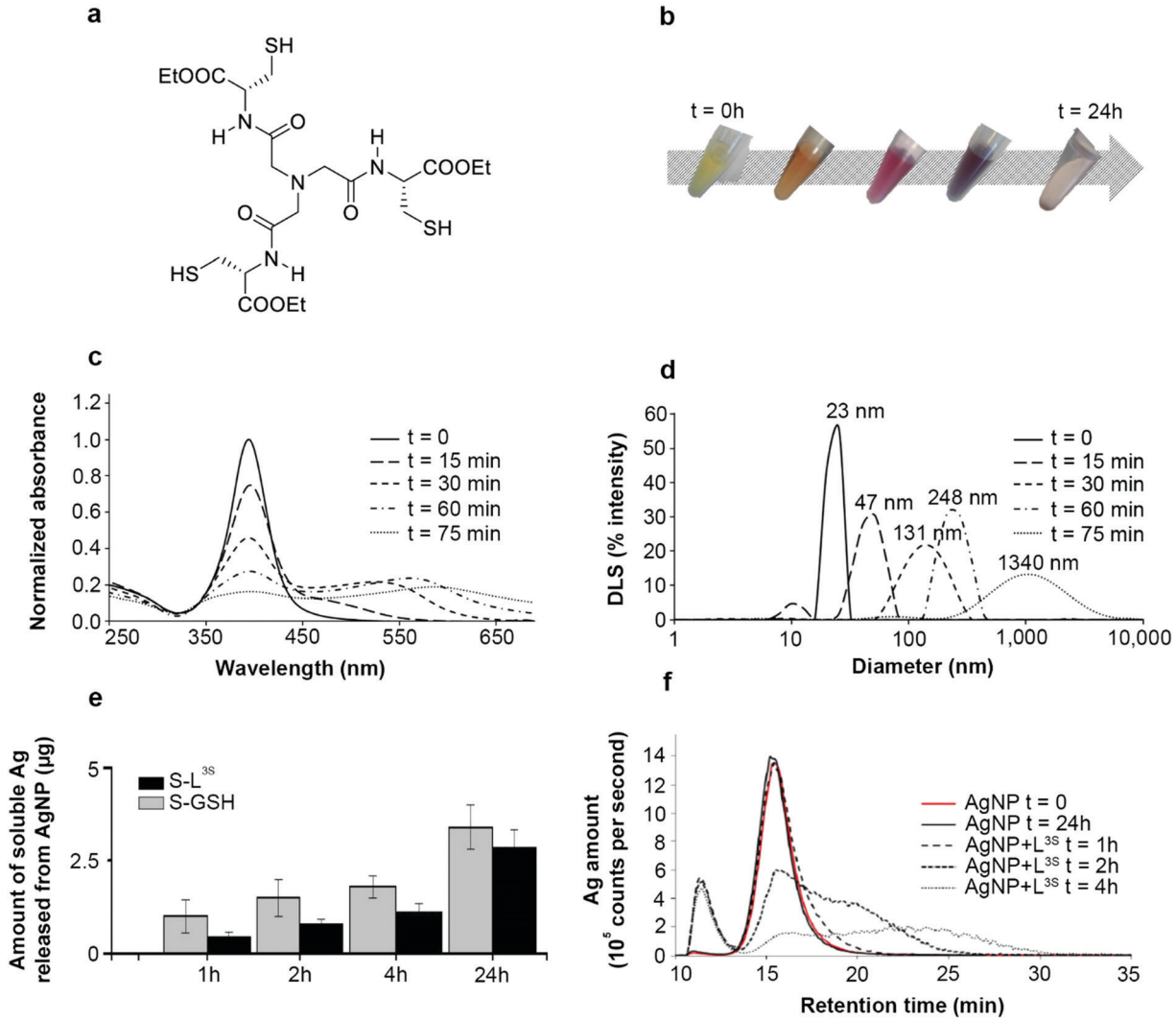

Fig. 1 L^{3S}-induced AgNP assemblies. (a) Chemical structure of the tripodal molecule L^{3S}. (b) Time-dependent evolution of the color of the AgNP–L^{3S} mixture between 0 and 24 hours. (c) Time-dependent analysis of AgNP SPR spectra in the presence of L^{3S} between 0 and 75 min of incubation at a S : Ag molar ratio of 1 : 1. (d) Time-dependent evolution of the hydrodynamic diameter distribution of the species in a solution containing AgNP and L^{3S} at a S : Ag molar ratio of 1 : 1 and between 0 and 75 min of incubation. The average diameter is written on top of each peak. (e) AgNP dissolution into Ag(I) species in the presence of GSH (denoted as "S-GSH") or L^{3S} (denoted as "S-L^{3S}"). Time-dependent measurement of the amount of Ag into the soluble fraction determined by ICP-AES. This amount corresponds to the fraction of the sample recovered in the supernatant of the sucrose cushion centrifugation (see Experimental section in ESI†). (f) AF_4 analysis of AgNPs in the presence of L^{3S}. Fractograms of species from AgNPs incubated alone for 0 or 24 hours and with L^{3S} for 1, 2 or 4 hours. The detection is based on ^{107}Ag by ICP-MS. In all experiments, t = 0 corresponds to the AgNP alone in solution.

larger the hydrodynamic diameter of an assembly the more diverse the possibilities to make it. Cryo-TEM also showed very short distances between AgNPs within an assembly, which is consistent with the small size of L^{3S} with maximum distances between two sulfur atoms in the nanometer range (Fig. 2d and Fig. S4c, ESI†). Thiols are at the core of the assembly mechanism, therefore we probed sulfur bonds with synchrotron radiation induced X-ray photoelectron spectroscopy (SR-XPS) on assemblies of small (40 nm diameter) and medium (80 nm diameter) sizes (Fig. 3). Between 56 and 64% of the sulfur atoms were found to be bound to Ag atoms at the NP surface, with two distinct geometries in similar proportions. S $2p_{3/2}$ components at binding energies (BE) of about 161 eV and 162 eV are attributed to sulfur atoms covalently bonded to metals in a monolayer or sub-monolayer regime, with the S atom in two different hybridizations, sp (161.3 eV) and sp^3 (162.1 eV),[16,17] coherently with what has already been observed for organic thiols chemisorbed onto gold surfaces.[18] The low BE signal is reported as occurring characteristically in self-assembling monolayers of low degree of coverage.[19] Indeed, a change in hybridization is likely to cause a peak shift,[20] with a BE of 162.1 eV for an sp^3 S atom, and a BE of about 161.3 eV (nearly 1 eV lower) would be expected for an sp-hybridized S atom.[20] This proves the direct binding of the thiolate functions of L^{3S} to the AgNP with two different geometries, linear and angular, corresponding to sp and sp^3 hybridization, respectively (Scheme S1, ESI†).[20,21] Due to the iodoacetamide reaction, 25 to 29% of the sulfur atoms were involved in bonds with carbon (thioethers), while the remaining 10 to 15% formed disulfide bridges.

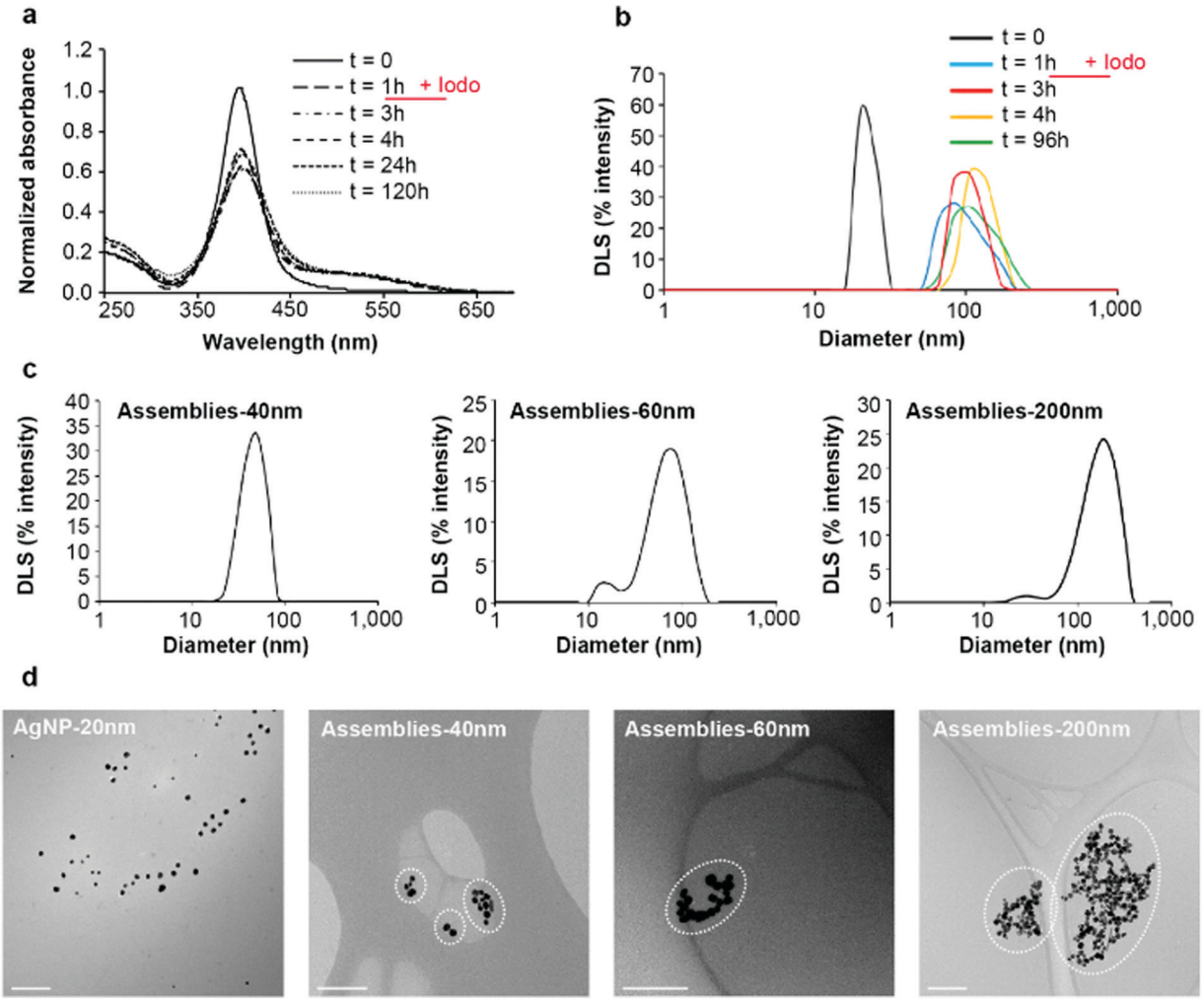

Fig. 2 AgNP assemblies: production, purification and characterization. (a) Time-dependent analysis of AgNP SPR spectra in the presence of L^{3S} between 0 and 120 hours of incubation at a S : Ag molar ratio of 0.25 : 1. The reaction between AgNPs and L^{3S} occurs for 1 hour, then iodoacetamide is added at 100 μM for a thiol concentration of 90 μM. SPR spectra were acquired up to 120 hours of the total incubation time. (b) In a set-up similar to (a), hydrodynamic diameter distribution of the species in solution was determined for the AgNPs alone (t = 0), at t = 1 h (time for the addition of iodoacetamide) and then at t = 3, 4 and 96 hours. (c) Hydrodynamic diameter distribution of different populations of assemblies separated by discontinuous sucrose gradient centrifugation. Three different populations were recovered: "Assemblies-40 nm" corresponds to assemblies of 40 nm average diameter by DLS, "Assemblies-60 nm" corresponds to assemblies of 60 nm average diameter by DLS and "Assemblies-200 nm" corresponds to assemblies of 200 nm average diameter by DLS. (d) Analysis by cryo-TEM of the different populations of assemblies compared to initial AgNPs, for which a proper dispersion on the grid is obtained. Assemblies composed of a larger number of particles with a larger diameter of the assemblies were observed on the grids. Clusters of AgNPs considered as an assembly are encircled to help the understanding of our statistical analysis (Fig. S4b, ESI†). The scale bar corresponds to 200 nm. "Iodo" stands for iodoacetamide.

This minor fraction of S species might belong to L^{3S} molecules grafted onto the NP surface with two thiolate groups, whereas the third thiolate forms an S–S bond with another partially grafted L^{3S} molecule. Besides, the absence of a signal component below 161 eV suggests that the assemblies do not contain silver sulfide.[25,27] XPS Ag 3d spectra showed that the fraction of Ag(I) remained constant around 6.6–6.8% of total Ag in the assemblies (Fig. S5, ESI†), which is close to the expected proportion of surface Ag for a 20 nm diameter NP (5.8%) confirming the limited dissolution of AgNPs. Therefore, AgNP assemblies are thiol-mediated and their structure is stabilized by Ag–S bonds involving L^{3S} that has the capability to bridge AgNPs thanks to its three thiol functions in a tripodal architecture. Besides, ToF-SIMS positive mode analysis enabled the detection of significant amounts of Ag atoms (both isotopes 107 and 109, Fig. S6, ESI†) for citrate-coated AgNPs but not for AgNP assemblies of 40 or 200 nm. Since ToF-SIMS information depth is limited to the first monolayers at the surface of the sample, these results showed that L^{3S} forms a layer that completely covers AgNPs in the assemblies.

The biological activity of assemblies of different diameters was then compared with citrated-coated AgNPs in order to gain insights into their potential as biocides and their toxicity for humans. All assemblies possess antibacterial activity against *Escherichia coli* (Gram-negative), with minimal inhibitory concentrations (MIC) of 5.2, 5.9 and 12.7 μM Ag for 40, 60 and 200 nm assemblies, respectively. These values are higher than

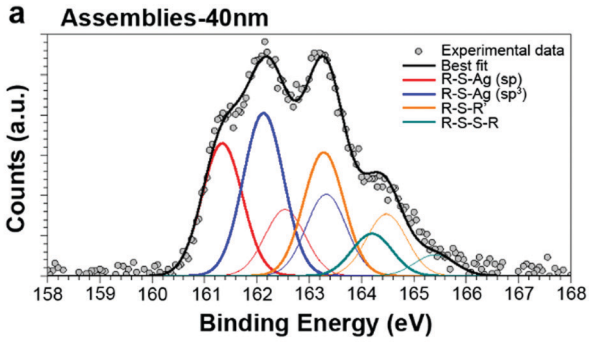

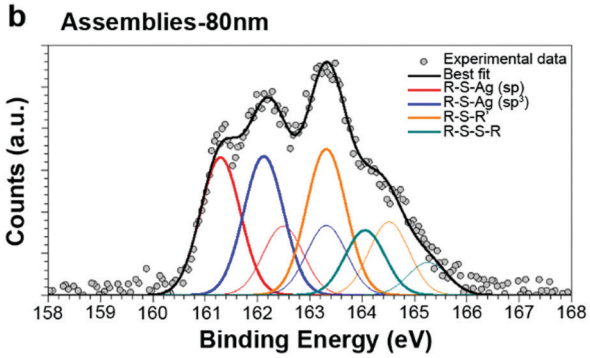

c

Assemblies	$S2p_{3/2}$ BE (eV)	FWHM (ev)	Atomic %*	Assignment
40 nm	161.33	0.83	29.4	**RS-Ag (sp)
	162.11	0.83	35.4	**RS-Ag (sp^3)
	163.20	0.83	24.8	RSR'
	163.92	0.83	10.4	RS-SR
80 nm	161.30	0.86	28.0	RS-Ag (sp)
	162.12	0.86	28.6	RS-Ag (sp^3)
	163.29	0.86	29.1	RSR'
	164.00	0.86	14.3	RS-SR

Fig. 3 Characterization of AgNP–L^{3S} interaction. SR-XPS S 2p core-level spectra collected on 40 nm AgNP assemblies (a) and 80 nm AgNP assemblies (b). For each signal, two spin–orbit components are reported: S $2p_{3/2}$ (thick curve) and S $2p_{1/2}$ (thin curve), with a fixed intensity ratio S $2p_{3/2}$/S $2p_{1/2}$ = 2/1 and doublet separation 1.2 eV. (c) Spectral assignment based on BE values of S $2p_{3/2}$ components and semiquantitative analysis resulting in the estimation of the relative amount of the identified S species. * the statistical error in semiquantitative XPS analysis is of about 5% of the estimated value,[22] ** as reported in ref. 16, 19, 20, 23–26.

a

Diameter (nm)	Object type	MIC – *E. coli* (μM Ag)	Growth delay – *B. subtilis* (μM Ag)
20	NP	0.7 +/- 0.0	260 +/- 89
40	NP	0.7 +/- 0.0	-
60	NP	2.9 +/- 0.0	-
40	Assemblies	5.2 +/- 3.2	113 +/- 75
60	Assemblies	5.9 +/- 3.6	138 +/- 48
200	Assemblies	12.7 +/- 1.0	33 +/- 14

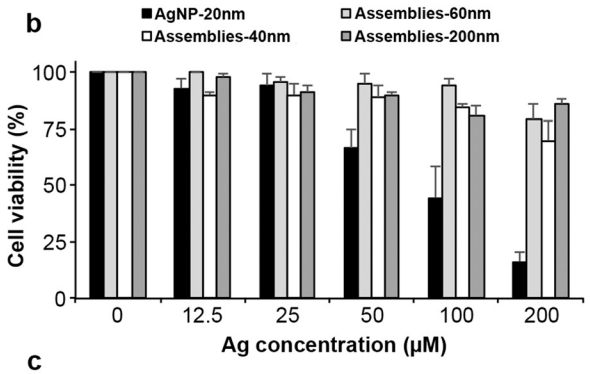

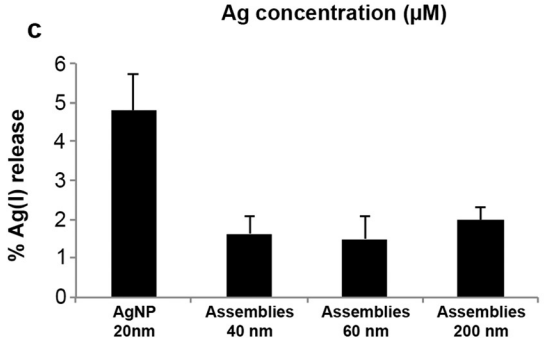

Fig. 4 Biological activity of AgNPs *versus* assemblies. (a) Table presenting the MIC for AgNPs and the different assemblies determined based on overnight growth in liquid minimal media for *E. coli* and the concentration inducing growth delay in LB medium for *B. subtilis*. (b) HepG2 cell viability. Hepatocytes were exposed to 20 nm citrate-coated AgNPs or assemblies of 40, 60 or 200 nm for 24 h before being harvested. Total and viable cells were counted in a TC20 Automated Cell Counter (Bio-Rad) using Trypan Blue. (c) Amount of Ag(I) released from AgNPs or assemblies in 10 days. Each sample diluted in HEPES–citrate buffer at 370 μM in Ag was incubated for 10 days at 25 °C with constant stirring at 400 rpm. The mixtures were separated by sucrose cushion centrifugation. Ag soluble species were in the supernatant and were quantified by ICP-AES. All the experiments were carried out at least three times independently.

those measured for citrate-coated 20 to 60 nm AgNPs (MIC between 0.7 and 2.9 μM) (Fig. 4a), but still much lower than the values reported in the literature for GSH-capped AgNPs (139 μM).[28] The biocidal activity was also tested against a Gram-positive bacterium, *Bacillus subtilis*, known to be difficult to kill by AgNPs notably because of its ability to modify the AgNP surface.[6,29] As expected, the Ag concentration required to observe a growth delay was much higher than that for *E. coli*: 113, 138 and 33 μM for assemblies of 40, 60 and 200 nm, respectively. Very interestingly, these concentrations are lower than the values determined for citrate-coated AgNPs (260 μM) (Fig. 4a). Therefore, the thick and tight coating afforded by the tri-thiol molecule L^{3S} may protect assemblies against AgNP surface modifications that could prevent biocidal activity, rendering our assemblies more robust. Besides, toxicity was assessed in the human hepatocarcinoma cell line HepG2 since AgNPs accumulate in the liver.[30] We were not able to reach a significantly toxic concentration (200 μM Ag higher concentration tested) for any of the assemblies, while the lethal dose for 50% of the cells is about 75 μM for citrate-coated AgNPs (Fig. 4b and Fig. S7, ESI†). Therefore, AgNP assemblies possess a biocidal activity against diverse strains but their cytotoxicity for eukaryote cells is drastically decreased.

Conclusions

In conclusion, we described an assembly mechanism of AgNPs bridged together by a bio-inspired tri-thiol molecule. This process, driven by thiol binding to surface Ag(I), results in the

formation of a scaffold that protects the NPs from massive transformations induced by various environmental conditions normally responsible for their fast dissolution, sulfidation or agglomeration (see review[5]). Moreover, these architectures do not prevent Ag(I) release but only slow it down (Fig. 4c), providing a nanomaterial that can be regarded as a novel promising safer-by-design biocide. Its tunable and controlled ion release and low sensitivity to the surrounding medium make it a long-lasting biocide with drastically reduced hazard for humans and the environment with respect to currently employed technologies. The controlled Ag(I) release cannot be explained only by surface coverage since PVP-coated AgNPs are more toxic for prokaryotes and eukaryotes than assemblies.[31] Therefore, the mixed sp^3–sp hybridization of L^{3S} thiols bound to surface Ag is likely to be responsible for the particular behavior of AgNPs involved in assemblies. The two hybridizations could mirror ligand binding on two different chemisorption sites, as hollow and on-top sites that favor stabilization of the assembly and dissolution into ions, respectively.[16,32]

The current work therefore describes the proof of concept for the development of novel biocidal AgNP assemblies. An original nanomaterial with promising properties has been developed thanks to a tripodal tri-thiol molecule, whose thiolate functions interact with surface Ag(I) ions, thereby bridging the NPs. Finally, further development of the organic molecule will enable the covalent grafting of the assemblies onto objects that require efficient and long-lasting biocides such as medical devices.

Author contributions

AD, IMS, PD and MM designed the study and interpreted the data. AD, GV, PD, IMS and MM wrote the paper. GV, IW and CB participated in data interpretation. MM, TG and IW characterized the assembly process and prepared AgNP assemblies. IW performed AF_4-ICP-MS experiments and interpreted the data. WLL performed cryo-TEM experiments including grid preparation. DL performed ToF-SIMS experiments and participated in data interpretation. CG synthesized the molecule L^{3S}. CB, LC, GV and MM participated in synchrotron XPS experiments, data acquisition and analysis, and interpretation of the results. PHJ and MM performed STEM experiments and analysis. MM and MC performed cellular experiments. MM and AD performed biocidal experiments.

Experimental section

Experimental details are available in the ESI.†

Conflicts of interest

There are no conflicts to declare.

Acknowledgements

The authors acknowledge Cécile Lelong for providing the *B. subtilis* strain, Delphine Truffier-Boutry for providing access to the AF_4 instrument and Elisabeth Mintz for discussions. This work was funded by the CEA-Toxicology Transversal Program through the NanoSilverSol grant and by the CEA Transversal Programs Toxicology and Nanoscience through the NanoTox-RX grant. This research is part of the LabEx ARCANE and CBH-EUR-GS (grant ANR-17-EURE-0003). This work is also a contribution to the Labex Serenade (ANR-11-LABX-0064) funded by the French Government's "Investissements d'Avenir" ANR program, through the A*MIDEX project (ANR-11-IDEX-0001-02). MM and IW were supported by the LabEx SERENADE. The research leading to these results has received funding from the European Community's Seventh Framework Programme (FP7/2007-2013) under grant agreement no. 312284. The authors acknowledge Igor Pis and Silvia Nappini for assistance in synchrotron-XPS measurements. The authors also acknowledge Alejandro Fernandez Martinez for his help with Zêta potential measurements that have been performed within the analytical platform of ISTerre (OSUG-France). The AF4-ICP-MS and NanoZS were funded by the EQUIPEX NanoID (grant ANR-10-EQPX-39-01). This work was also supported by the Université Grenoble Alpes – AGIR grant NanoSilverSafe and IRS NanoBIS grant. This work used the electron microscope platform of the Grenoble Instruct-ERIC Center (ISBG: UMS 3518 CNRS-CEA-UGA-EMBL) with support from FRISBI (ANR-10-INBS-05-02) and GRAL (ANR-10-LABX-49-01) within the Grenoble Partnership for Structural Biology (PSB). The EM facility is supported by the Auvergne-Rhône-Alpes Region, the Fondation Recherche Medicale (FRM), the fonds FEDER and the GIS-Infrastrutures en Biologie Sante et Agronomie (IBISA). We thank Dr Guy Schoehn for support and access to the EM platform.

Notes and references

1 C. Gunawan, C. P. Marquis, R. Amal, G. A. Sotiriou, S. A. Rice and E. J. Harry, *ACS Nano*, 2017, **11**, 3438–3445.
2 C. Haefeli, C. Franklin and K. Hardy, *J. Bacteriol.*, 1984, **158**, 389–392.
3 S. Silver, *FEMS Microbiol. Rev.*, 2003, **27**, 341–353.
4 S. Silver, A. Gupta, K. Matsui and J.-F. Lo, *Met.-Based Drugs*, 1999, **6**, 315–320.
5 M. Marchioni, P.-H. Jouneau, M. Chevallet, I. Michaud-Soret and A. Deniaud, *Coord. Chem. Rev.*, 2018, **364**, 118–136.
6 E. Eymard-Vernain, Y. Coute, A. Adrait, T. Rabilloud, G. Sarret and C. Lelong, *PLoS One*, 2018, **13**, e0197501.
7 J. Liu and R. H. Hurt, *Environ. Sci. Technol.*, 2010, **44**, 2169–2175.
8 J. Liu, D. A. Sonshine, S. Shervani and R. H. Hurt, *ACS Nano*, 2010, **4**, 6903–6913.
9 M. Marchioni, T. Gallon, I. Worms, P.-H. Jouneau, C. Lebrun, G. Veronesi, D. Truffier-Boutry, E. Mintz, P. Delangle, A. Deniaud and I. Michaud-Soret, *Environ. Sci.: Nano*, 2018, **5**, 1911–1920.
10 L. Sigg and U. Lindauer, *Environ. Pollut.*, 2015, **206**, 582–587.
11 F. Porcaro, L. Carlini, A. Ugolini, D. Visaggio, P. Visca, I. Fratoddi, I. Venditti, C. Meneghini, L. Simonelli, C. Marini, W. Olszewski, N. Ramanan, I. Luisetto and C. Battocchio, *Materials*, 2016, **9**, 1028.

12 J. Y. Bottero, J. Rose, C. de Garidel, A. Masion, T. Deutsch, G. Brochard, M. Carrière, N. Gontard, H. Wortham, T. Rabilloud, B. Salles, M. Dubosson, B. Cathala, D. Boutry, A. Ereskovsky, C. Auplat, L. Charlet, T. Heulin, E. Frejafon and S. Lanone, *Environ. Sci.: Nano*, 2017, **4**, 526–538.
13 A. M. Pujol, C. Gateau, C. Lebrun and P. Delangle, *J. Am. Chem. Soc.*, 2009, **131**, 6928–6929.
14 G. Veronesi, T. Gallon, A. Deniaud, B. Boff, C. Gateau, C. Lebrun, C. Vidaud, F. Rollin-Genetet, M. Carrière, I. Kieffer, E. Mintz, P. Delangle and I. Michaud-Soret, *Inorg. Chem.*, 2015, **54**, 11688–11696.
15 H. Cha, D. Lee, J. H. Yoon and S. Yoon, *J. Colloid Interface Sci.*, 2016, **464**, 18–24.
16 I. Venditti, G. Testa, F. Sciubba, L. Carlini, F. Porcaro, C. Meneghini, S. Mobilio, C. Battocchio and I. Fratoddi, *J. Phys. Chem. C*, 2017, **121**, 8002–8013.
17 F. Mochi, L. Burratti, I. Fratoddi, I. Venditti, C. Battocchio, L. Carlini, G. Iucci, M. Casalboni, F. De Matteis, S. Casciardi, S. Nappini, I. Pis and P. Prosposito, *Nanomaterials*, 2018, **8**, 488.
18 S. Ramsaywack, S. Martić, S. Milton, L. Gates, A. S. Grant, M. Labib, A. Decken and H.-B. Kraatz, *J. Phys. Chem. C*, 2012, **116**, 7886–7896.
19 T. Ishida, M. Hara, I. Kojima, S. Tsuneda, N. Nishida, H. Sasabe and W. Knoll, *Langmuir*, 1998, **14**, 2092–2096.
20 A. J. Leavitt and T. P. Beebe Jr, *Surf. Sci.*, 1994, **314**, 23–33.
21 T. Ishida, N. Choi, W. Mizutani, H. Tokumoto, I. Kojima, H. Azehara, H. Hokari, U. Akiba and M. Fujihira, *Langmuir*, 1999, **15**, 6799–6806.
22 J. E. Castle, *Surf. Interface Anal.*, 1984, **6**, 302.
23 N. Nishida, M. Hara, H. Sasabe and W. Knoll, *Jpn. J. Appl. Phys.*, 1996, **35**, 5866.
24 G. Beamson and D. Briggs, *High resolution XPS of organic polymers: the Scienta ESCA300 database*, Wiley, Chichester [England], New York, 1992.
25 A. V. Naumkin, A. Kraut-Vass, S. W. Gaarenstroom and C. J. Powell, NIST X-ray Photoelectron Spectroscopy Database, Version 4.1, National Institute of Standards and Technology, Gaithersburg, 2013.
26 B. J. Lindberg, K. Hamrin, G. Johansson, U. Gelius, A. Fahlman, C. Nordling and K. Siegbahn, *Phys. Scr.*, 1970, **1**, 286.
27 C. Battocchio, C. Meneghini, I. Fratoddi, I. Venditti, M. V. Russo, G. Aquilanti, C. Maurizio, F. Bondino, R. Matassa and M. Rossi, *J. Phys. Chem. C*, 2012, **116**, 19571–19578.
28 E. Amato, Y. A. Diaz-Fernandez, A. Taglietti, P. Pallavicini, L. Pasotti, L. Cucca, C. Milanese, P. Grisoli, C. Dacarro, J. M. Fernandez-Hechavarria and V. Necchi, *Langmuir*, 2011, **27**, 9165–9173.
29 K. Rafińska, P. Pomastowski and B. Buszewski, *Sci. Total Environ*, 2019, **661**, 120–129.
30 M. van der Zande, R. J. Vandebriel, E. Van Doren, E. Kramer, Z. Herrera Rivera, C. S. Serrano-Rojero, E. R. Gremmer, J. Mast, R. J. B. Peters, P. C. H. Hollman, P. J. M. Hendriksen, H. J. P. Marvin, A. A. C. M. Peijnenburg and H. Bouwmeester, *ACS Nano*, 2012, **6**, 7427–7442.
31 G. Veronesi, A. Deniaud, T. Gallon, P.-H. Jouneau, J. Villanova, P. Delangle, M. Carrière, I. Kieffer, P. Charbonnier, E. Mintz and I. Michaud-Soret, *Nanoscale*, 2016, **8**, 17012–17021.
32 H. Sellers, A. Ulman, Y. Shnidman and J. E. Eilers, *J. Am. Chem. Soc.*, 1993, **115**, 9389–9401.